Influence of the Solvent on the Self-Assembly of a Modified Amyloid Beta Peptide Fragment. I. Morphological Investigation

V. Castelletto* and I. W. Hamley*

Dept of Chemistry, The University of Reading, Reading RG6 6AD, U.K.

P. J. F. Harris

Centre for Advanced Microscopy, The University of Reading, Reading RG6 6AF, U.K.

U. Olsson

Physical Chemistry 1, Lund University, S-221 00 Lund, Sweden

N. Spencer

The Biocentre, The University of Reading, Reading RG6 6AS, U.K.

Received: March 30, 2009; Revised Manuscript Received: May 8, 2009

The solvent-induced transition between self-assembled structures formed by the peptide AAKLVFF is studied via electron microscopy, light scattering, and spectroscopic techniques. The peptide is based on a core fragment of the amyloid β-peptide, KLVFF, extended by two alanine residues. AAKLVFF exhibits distinct structures of twisted fibrils in water or nanotubes in methanol. For intermediate water/methanol compositions, these structures are disrupted and replaced by wide filamentous tapes that appear to be lateral aggregates of thin protofilaments. The orientation of the β-strands in the twisted tapes or nanotubes can be deduced from X-ray diffraction on aligned stalks, as well as FT-IR experiments in transmission compared to attenuated total reflection. Strands are aligned perpendicular to the axis of the twisted fibrils or the nanotubes. The results are interpreted in light of recent results on the effect of competitive hydrogen bonding upon self-assembly in soft materials in water/methanol mixtures.

1. Introduction

The self-assembly of model peptides into fibril containing β-sheets is of great interest due to its relevance to amyloid diseases such as Alzheimer's[1,2] and also due to the potential applications of peptide fibrils as structural elements in advanced biomaterials.[3,4]

We have recently been investigating the self-assembly of peptides based on a core sequence of the amyloid β (Aβ)-peptide. The Aβ-peptide is implicated in Alzheimer's and is cleaved in vivo from a larger precursor protein to form fragments with predominantly 40 or 42 residues.[2,5,6] We have focused on the sequence KLVFF, corresponding to Aβ16−20.[6] We have also prepared variants of KLVFF extended at the N-terminus with additional hydrophobic residues in order to investigate the role of hydrophobic and aromatic interactions on peptide self-assembly. In particular, we have examined the fibrillization of FFKLVFF in methanol since the peptide is too hydrophobic to dissolve in water and found evidence for β-sheet self-assembly.[7] We propose that this is driven in large part by aromatic interactions between F residues, as confirmed by UV (ultraviolet) and CD (circular dichroism) spectroscopy. A sample with nonaromatic residues at one terminus, AAKLVFF, has very interesting self-assembly properties, forming distinct structures in solvents with different polarity. When dissolved in methanol, AAKLVFF self-assembles into nanotubes, which can form a nematic phase at sufficiently high concentration.[8] In water, AAKLVFF forms very well ordered fibrils.[9]

Peptide NH_2−AAKLVFF−COOH is related to Aβ16−22, Ac−KLVFFAE−NH_2, studied by Lynn and co-workers[10,11] in the sense that both are heptamers containing KLVFF. In our case, KLVFF is extended by two alanine residues at the N-terminus, and furthermore, the termini are charged because the peptide is not capped. In contrast, Aβ16−22 studied by Lynn and co-workers is capped but contains the ionic glutamic acid residue E as well as the basic residue lysine K. This gives rise to pH-dependent self-assembly properties. At pH 2, where both K and E are expected to be protonated and the peptide has a single positive charge, nanotubes are observed.[10,11] In contrast, at pH 6, there is a positive charge at the N-terminus and a negative charge at the C-terminus, and homogeneous fibrils are observed. Antiparallel β-strand registry was distinct in nanotube and fibril structures, as revealed by Fourier transform infrared spectroscopy (FT-IR) in the amide I region and solid-state NMR, both using peptides containing labeled L or A residues (the fiber XRD pattern was also distinct for fibrils and nanotubes).[10] Cross-strand pairwise interactions were shown to contribute to the self-assembly process, studied via FT-IR on V18 variants and molecular dynamics simulations.[10] Pairwise electrostatic interactions between K and E and also the packing of the β-carbon in V dictate the peptide backbone registry.[11]

The present paper is focused on an investigation of the transition between nanotubes of AAKLVFF in methanol and

* To whom correspondence should be addressed. Tel: 44 118 378 4746. Fax: 44 118 378 6331. E-mail: V.Castelletto@reading.ac.uk (V.C.); Tel: 44 118 378 6341. Fax: 44 118 378 6331. E-mail: I.W.Hamley@reading.ac.uk (I.W.H.).

10.1021/jp902860a CCC: $40.75
Published on Web 06/25/2009

fibrils in water. Our focus is therefore on the influence of solvent polarity on self-assembly, rather than solution pH, as in the work of Lynn and co-workers. Water and methanol are both polar solvents, capable of hydrogen bonding but with different relative permittivity. The composition of water/methanol mixtures is varied, and the self-assembly and secondary structure are probed using a combination of transmission electron microscopy (TEM), fiber X-ray diffraction (XRD), circular dichroism (CD), and FT-IR. As noted elsewhere,[12] differences in the morphology of amyloid peptide fibrils can lead to differences in neurotoxicity[13] and the propagation of the fibrils,[13] as well as distinct phenotypes resulting from the mode of the self-assembly.[14] It is therefore of great interest to understand the origin of different self-assembled structures in model amyloid peptide fibrils such as AAKLVFF.

2. Experimental Section

Materials. AAKLVFF was custom synthesized by C.S. Bio Company (U.S.A.) and was used as received, without further purification. Solutions were made using different amounts of peptide and different fractions of methanol to Millipore filtered water. The solutions were mixed and left to rest at least for the following hour before collecting experimental data. The fraction of methanol to water in the solution was calculated as a weight percent, according to [(weight of methanol × 100/weight of (methanol + water)) wt %]. Samples containing 0 wt % methanol had pH 3, while samples with 20−100 wt % methanol had pH 5.

TEM. TEM experiments were performed using a Philips CM20 transmission electron microscope operated at 80 kV, while high-resolution TEM (HR-TEM) was done using a JEOL JEM-2010 microscope operated at 100 kV. Droplets of the peptide solution (0.45 wt % AAKLVFF containing 100 wt % methanol or 1 wt % AAKLVFF containing 0−70 wt % methanol) were placed on Cu grids coated with a carbon film (Agar Scientific, U.K.), stained with uranyl acetate (1 wt %) (Agar Scientific, U.K.), and dried.

Cryo-TEM. Experiments were performed using a Philips CM 120 Bio-Twin transmission electron microscope. A small quantity of sample was placed on a copper grid in a thermostatted chamber at 25 °C. The sample in the grid was then blotted to create a thin film. Afterward, the copper grid with the sample was quickly vitrified by immersion in liquid ethane[15] and carefully transferred under a liquid nitrogen environment to the microscope.

DLS. Experiments were performed using an ALV CGS-3 system with a 5003 multidigital correlator. The light source was a 20 mW He−Ne laser, linearly polarized, with $\lambda = 633$ nm. Scattering angles in the range of $40 \leq \theta \leq 150°$ were used for all of the experiments. Samples containing 0.5 wt % AAKLVFF and 0−100 wt % methanol were filtered through 0.20 μm Anotop filters from Whatman into standard 0.5 cm diameter cylindrical glass cells. The time evolution of the DLS data was studied for the sample with 20 wt % methanol immediately after filtration, while the DLS for samples with 0 and 40−100 wt % methanol were measured ∼3 h after each sample was filtered to allow for equilibration of the solution structure.

DLS experiments measured the intensity correlation function of the scattered light $g^{(2)}(q,t)$[16]

$$g^{(2)}(q,t) = 1 + A[g^{(1)}(q,t)]^2 \tag{1}$$

where A is a correction factor depending on the alignment of the instrument, $q = [4\pi n \sin(\theta/2)]/\lambda$ is the scattering vector (n = refractive index of the medium), t is the delay time, and $g^{(1)}(q,t)$ is the electric field correlation function.

The relaxation rate distribution of the system can be calculated by inverting the field correlation function $G(\Gamma)$[17]

$$g^{(1)}(t) = \int_0^\infty G(\Gamma) \exp(-\Gamma t) d\Gamma \tag{2}$$

The inverse Laplace transform of eq 2 provides a tool for calculating $G(\Gamma)$ and therefore the diffusion coefficients of the system. Alternatively, the distribution function G in eq 2 can be written as a function of the particle radius. Any apparent hydrodynamic radius of the system, $\langle R_h \rangle_{z,app}$, is taken as the radius corresponding to a maximum in $G(\langle R_h \rangle_{z,app})$. In this work, a constrained regularization method included in the ALV-5000/E for WINDOWS software was used to calculate $G(\langle R_h \rangle_{z,app})$ for $\theta = 90°$. The same software was used to calculate $\langle R_h \rangle_{z,app}$ using a cumulant analysis. In this method, the analysis of the cumulant expansion of the correlation function is done by fitting a polynomial function according to

$$\ln(g^{(1)}(q,t)) = \ln(X) + \langle \Gamma \rangle t + \frac{\mu_2}{2} t^2 - \frac{\mu_3}{6} t^3 \tag{3}$$

where the fitting parameters are the amplitude (X), the characteristic time ($1/\langle \Gamma \rangle$; $\langle \Gamma \rangle$ = initial decay rate), and the coefficients μ_2 and μ_3.

The apparent hydrodynamic radius of the system, $\langle R_h \rangle_{z,app}$, is calculated from $\langle \Gamma \rangle$ through the equation

$$\langle R_h \rangle_{z,app} = \frac{k_B T}{6\pi\eta_0 \langle \Gamma \rangle} q^2 \tag{4}$$

where $k_B = 1.38 \times 10^{-23}$ J K^{-1} is the Boltzmann constant, η_0 is the viscosity of the solvent, and T is the temperature. The viscosities $\eta_0 = 0.89$, 1.34, 1.56, 1.54, 1.30, and 0.55 cP were used for 0, 20, 40, 50, 70, and 100 wt % methanol, respectively.[18]

Murphy and co-workers[19] have already shown that in the case of amyloid fibers, it is possible to estimate the length of the fiber (L_{DLS}) using the q dependence of $\langle \Gamma \rangle$. They applied the expression derived by Maeda and Fujime[20] for $\langle \Gamma \rangle / q^2$ for a solution of rigid rods

$$\frac{\langle \Gamma \rangle}{q^2} = \varepsilon \qquad (qL_{DLS} \ll 1) \tag{5}$$

where ε is the translational diffusion coefficient.

Following Murphy and co-workers' methodology, it is then possible to apply the Broersma equations[21] to calculate ε as a function of the rod length L_{DLS} and thickness D

$$\begin{aligned} \varepsilon &= \frac{k_B T}{3\pi\eta_0 L_{DLS}} \left[\delta - \frac{1}{2}(\gamma_1 + \gamma_3) \right] \\ \delta &= \ln\left(\frac{2L_{DLS}}{D}\right) \\ \gamma_1 &= 0.19 - 4.2(\delta^{-1} - 0.39)^2 \\ \gamma_2 &= 1.27 - 7.4(\delta^{-1} - 0.34)^2 \end{aligned} \tag{6}$$

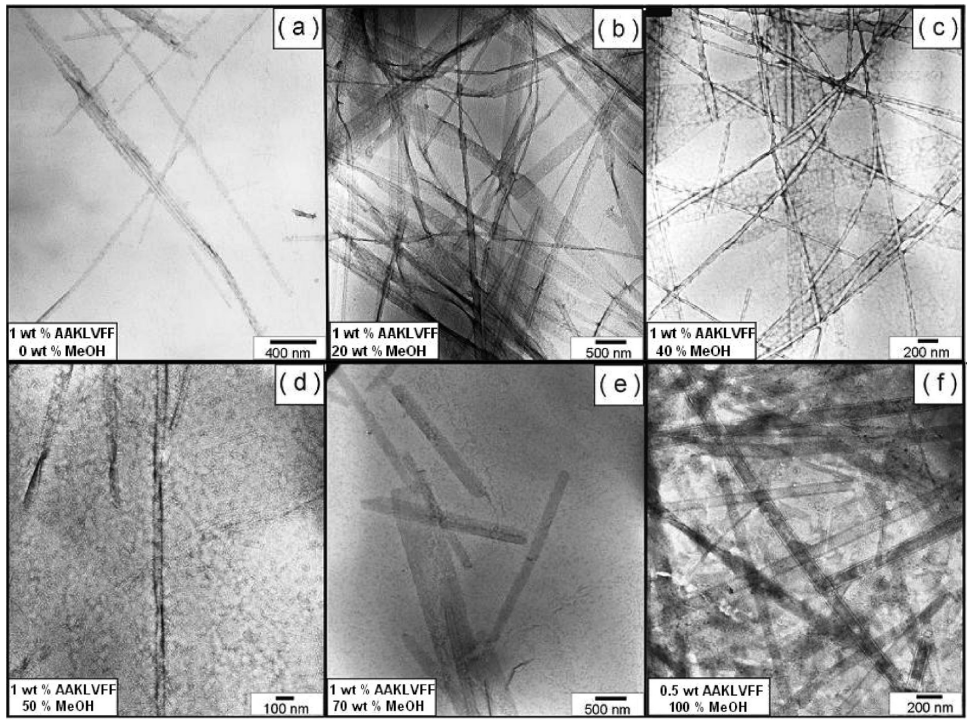

Figure 1. TEM images obtained for films dried from 1 wt % AAKLVFF solutions containing (a) 0, (b) 20, (c) 40, (d) 50, (e) 70, and (f) 100 wt % methanol.

SLS. Static light scattering was performed using a custom-built instrument described elsewhere.[22] Briefly, it comprises a He−Ne laser, optics train, a sample contained in a Linkam CSS 450 shear cell, a diffuser plate, and a CCD camera to detect images. The sample was subjected to a range of shear rates; however, no significant orientation was observed, and therefore, the two-dimensional patterns obtained were integrated to one-dimensional profiles of intensity versus scattering angle and hence wavenumber q (calibrated using a diffraction grating).

Circular Dichroism. The CD spectra were recorded on a Chirascan spectropolarimeter (Applied Photophysics, U.K.). Peptide solutions with different contents of methanol (0.03 wt % AAKLVFF containing 20−100 wt % methanol) were loaded into 1 mm quartz cells. Dried films obtained from 0.5 wt % peptide solutions containing 20−100 wt % methanol were also prepared on a glass plate and studied by CD. Spectra were obtained from 200 to 260 nm with a 0.5 nm step and 1 s collection time per step at 20 °C, taking five averages.

FT-IR. Spectra were recorded using a Nexus-FT-IR spectrometer equipped with a DTGS detector and a multiple reflection ATR system. Transmission FT-IR measurements were performed using a CaF_2 plate, while grazing angle FT-IR experiments were done using a ZnSe plate. For both transmission and grazing angle configurations, small aliquots of AAKLVFF solutions (1 wt % AAKLVFF containing 40−100 wt % methanol) were deposited on the corresponding plate and allowed to dry, providing a solid film of dry peptide. Spectra were scanned 64 and 128 times for transmission and grazing angle geometries, respectively. Sample solutions in D_2O and methanol-$d4$ (1 wt % AAKLVFF containing 20−100 wt % methanol) were sandwiched between two CaF_2 plate windows (spacer 0.006 mm) and studied by transmission FT-IR. Spectra were scanned 128 times.

XRD. X-ray diffraction was performed on stalks prepared by drying filaments of the peptide. Solutions containing 1 wt % AAKLVFF and 20−100 wt % methanol were suspended in between the ends of wax-coated capillaries and dried. The stalks were mounted (vertically) onto the four axis goniometer of a RAXIS IV++ X-ray diffractometer (Rigaku) equipped with a rotating anode generator. The XRD data were collected using a Saturn 992 CCD camera.

3. Results and Discussion

The self-assembled morphology of AAKLVFF in water/methanol mixtures was studied by TEM, HR-TEM, cryo-TEM, DLS, and SLS. In a second stage, the secondary structure of AAKLVFF fibrils and nanotubes was assessed using CD, FT-IR, and XRD. The presentation of our results starts with TEM and light scattering studies of the self-assembled structure, followed by the spectroscopy results on the secondary structure.

Self-Organization of AAKLVFF. Solutions containing 0.45 or 1 wt % AAKLVFF with 0−100 wt % methanol were studied by TEM and HR-TEM. Figure 1a−f shows some representative TEM images for the corresponding dried films.

The TEM images in Figure 1 reveal three different species. These consist of nanotubes, thin fibrils, and thick tapes made by the self-assembly of the thin fibrils (in a side-by-side configuration). TEM allowed the diameter of the fibril or nanotubes, D_{TEM}, to be determined, as well as the thickness of the nanotube wall, W_{TEM}. However, only the lower limit to the length of the fibril or nanotubes, L_{TEM}, could be determined by TEM. The values for the parameters D_{TEM}, W_{TEM}, and L_{TEM} obtained from Figure 1 are listed in Table 1.

Figure 1a corresponds to a dried film of 1 wt % AAKLVFF with 0 wt % methanol. The TEM for this sample has been extensively discussed by us in a previous work[9] and is shown here only as a reference. The fibrils in this sample are highly flexible. Some of the fibrils are joined together in tapes, such that thinner tapes are twisted, denoting a degree of flexibility.

The dried film obtained from a solution containing 20 wt % methanol (Figure 1b) shows thin twisted fibrils coexisting with wide flat tapes. In certain places, twist of the tapes is observed.

The film corresponding to 40 wt % methanol (Figure 1c) also indicates coexistence of twisted fibrils and flat tapes. We believe

TABLE 1: Structural Parameters of the Individual Fibrils, Tapes, or Nanotubes Measured by TEM, Cryo-TEM and DLS[a]

wt % methanol	D_{TEM}/nm	W_{TEM}/nm	L_{TEM}/μm	D_{cryo}/nm	W_{cryo}/nm	L_{cryo}/μm	L_{DLS}/μm
0	$(26 \pm 5)^f$		$(5)^f$	$(18.5 \pm 3.3)^f$		$(4)^f_{day\ 1}$ $(5)^f_{day\ 22}$	85
20	$(53 \pm 13)^f$		$(5)^f$				
40	$(40 \pm 10)^f$						
50	$(54 \pm 7)^f$		$(2)^f$	$(63.8 \pm 10.3)^f$			
70	$(332 \pm 147)^t$			$(133.9 \pm 35.5)^f$ $(569 \pm 310)^t$			2.7
100	$(104.4 \pm 13.5)^n$	$(7.9 \pm 1.7)^n$	$(3.5)^n$	$(85.5 \pm 8.4)^n$	$(5.3 \pm 0.3)^n$	$(3.2)^n$	3.2

[a] Variables: thickness, D; lower length limit, L; nanotube wall thickness, W. The superscripts f, t, or n indicate a fibril, tape, or nanotube, respectively. The subscripts TEM, cryo-TEM, or DLS denote the technique.

that the perpendicular "bamboo" features on the fibril (Figure 1c) are cracks resulting from sample drying.

Figure 1d shows that a dry film from the 50 wt % methanol solution contains only twisted fibrils. The film dried from a solution containing 70 wt % methanol (Figure 1e, Table 1) does not present peptide fibrils. Instead, the sample appears to show highly polydisperse homogeneous stiff tapes.

Figure 1f, obtained from a 0.45 wt % AAKLVFF solution in methanol, clearly shows the existence of nanotubes. The nanotube parameters obtained from Figure 1e (Table 1) are consistent with a width of 116 ± 16 nm, a wall thickness of $\sim$3.5 nm, and $L \geq 1$ μm, previously reported by us for AAKLVFF nanotubes in methanol obtained using an in-house-synthesized peptide.[8]

The TEM images indicate that the flexibility of the AAKLFFF fibers is not affected significantly by a solution composition < 70 wt % methanol. This is not valid for solutions containing 70 wt % methanol or more, where fibrils are absent and replaced by stiff wide tapes or nanotubes.

It can be concluded at this stage that samples containing 0−50 wt % methanol contain flexible individual fibrils with a width in the narrow range of 26−54 nm (Table 1). Stiff homogeneous tapes, 332 nm wide, are observed for 70 wt % methanol. Peptide nanotubes, with a 104 nm diameter, are formed only for 100 wt % methanol (Table 1).

Figure 1d shows that the dried film for the sample containing 50 wt % methanol does not reveal the presence of flat tapes observed for 0−40 and 70 wt % methanol, at least in the area investigated in the TEM grid. Indeed, the formation of flat tapes does not seem to depend on the methanol content. It might be associated with a nonequilibrium effect or a drying effect. However, cryo-TEM, FT-IR, and XRD on samples dried from mixed solvents (vide infra) suggest that at the supramolecular and the molecular level, drying does not appreciably influence the structure of aggregates of AAKLVFF.

Cryo-TEM experiments were performed in order to evaluate the influence of drying effects on the TEM samples and to check whether the structures observed by TEM are preserved in solution. Samples containing 1 wt % AAKLVFF and 0, 50, 70, and 100 wt % methanol were studied by cryo-TEM. The results are shown in Figures 2 and 3.

Similarly to the TEM images in Figure 1, the cryo-TEM images reveal the formation of fibrils, tapes, and nanotubes. The width of the fibrils or nanotubes, D_{cryo}, as well as the thickness of the nanotube wall, W_{cryo}, and the lower limit to the length of the fibrils or nanotubes, L_{cryo}, obtained from Figures 2 and 3 are listed in Table 1.

Figure 2 shows the cryo-TEM results obtained for a sample containing 1 wt % AAKLVFF with 0 wt % methanol. Figure 2a,b corresponds to the fresh sample, while Figure 2c,d correspond to the same sample aged for 22 days. Figure 2 shows

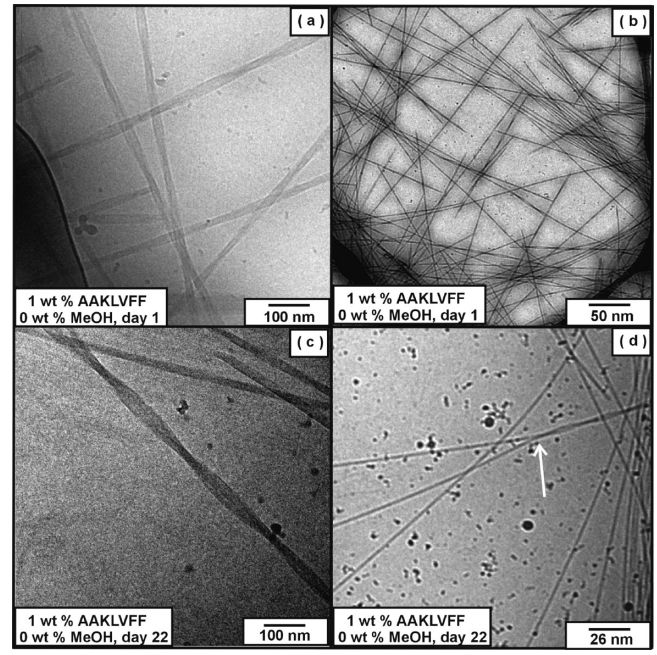

Figure 2. Cryo-TEM images obtained for 1 wt % AAKLVFF solutions containing 0 wt % methanol (a,b) within 1 day after sample preparation and (c,d) 22 days after sample preparation. The white arrow in (d) shows the position where two fibrils become twisted together around a common axis.

that both the fresh sample and the aged sample contain fibrils with the same average thickness (Table 1). Individual fibrils or bundles of 2−3 fibrils (Figure 2a−d) are twisted around the main fibril axis. The difference between fresh fibrils and mature fibrils is apparently mainly in their length since the fibril length in the fresh samples appears shorter than that in the aged sample (Figure 2b,d, Table 1).

Figure 3 shows the cryo-TEM obtained for 1 wt % solutions of AAKLVFF with 50, 70, or 100 wt % methanol.

The cryo-TEM image in Figure 3a (1 wt % AAKLVFF, 50 wt % methanol) shows the formation of highly polydisperse flexible tapes. These wide tapes seem to comprise homogeneous individual fibrils stacked side by side.

Figure 3b shows the results for 1 wt % AAKLVFF containing 70 wt % methanol. The formation of wide tapes composed of thinner fibrils (Table 1) is also observed for this sample. The wide tapes are more rigid than those observed for 50 wt % methanol. Their width is listed in Table 1 to enable the comparison with the similar data obtained from the TEM image (Figure 1e). Nanotubes are clearly revealed in the cryo-TEM for the methanol solution (Figure 3c,d).

From the analysis of the results from TEM and cryo-TEM presented in Figures 1−3, it is possible to conclude that the general features of the self-assembled structure formed by

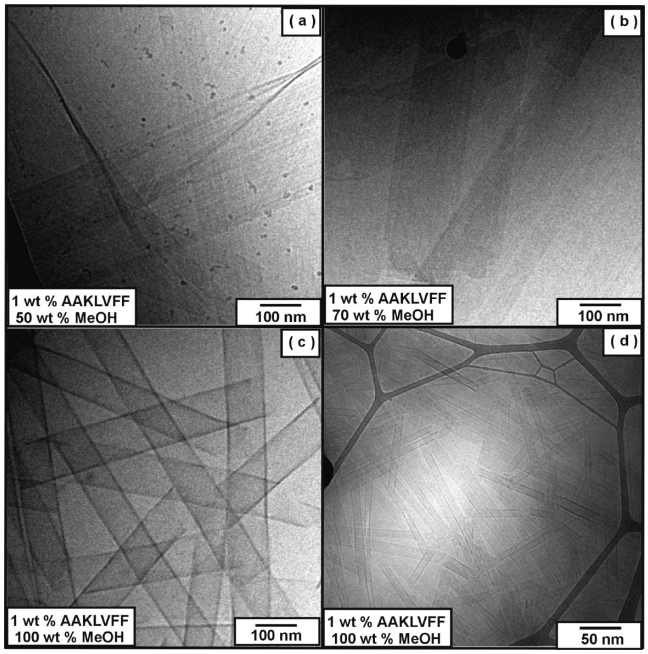

Figure 3. Cryo-TEM images obtained for 1 wt % AAKLVFF solutions containing (a) 50, (b) 70, and (c,d) 100 wt % methanol.

AAKLVFF in solution is preserved in the dried film. The diameter of the individual fibrils (for 0, 50, 70, and 100 wt % methanol) is comparable for both techniques. AAKLVFF is apparently a sufficiently strong fibrillizing peptide for the self-assembled structure not to be disrupted upon drying, in contrast to the weak fibrillizing peptide KLVFF.[6]

DLS experiments were undertaken in order to examine the dimensions of self-assembled structures in solutions containing 0.5 wt % AAKLVFF and different solvent compositions.

The constrained regularization method was used to calculate the distribution of hydrodynamic radii for samples containing 0−100 wt % methanol (Figure 4a). The hydrodynamic radii extracted from each distribution are plotted in Figure 4b as a function of the methanol content of the sample. The hydrodynamic radii obtained can be can be grouped into three average values corresponding to $\overline{\langle R_h \rangle}_{z,app}$ 690, 30, and 0.7 nm.

According to Figure 4a, the main contribution to the light scattering data is from structures with $\langle R_h \rangle_{z,app} = 453-692$ nm ($\overline{\langle R_h \rangle}_{z,app}$ 690 nm). We associate this with the fibrillar and nanotube structures as a whole, apparent in the TEM images. We have previously reported $\langle R_h \rangle_{z,app} = 600$ nm for 0.5 wt % AAKLVFF in methanol,[8] similar to the value shown in Figure 4b.

The small peak in the $R_{H,app}$ distribution functions with $\overline{\langle R_h \rangle}_{z,app}$ 0.7 nm lies outside of limits of detection of the instrument; therefore, it will not be taken into consideration for our analysis. Comparison to the D values listed in Table 1 suggests that the peak with $\overline{\langle R_h \rangle}_{z,app} = 29$ nm might be assigned to the width of the peptide fibers or nanotubes.

The cumulant analysis was also used as an alternative method to calculate the hydrodynamic radii of the system since it avoids mathematical artifacts due to the regularization method. The calculated radii are plotted in Figure 4b, together with $\langle R_h \rangle_{z,app}$ calculated by the constrained regularization method. As expected, $\langle R_h \rangle_{z,app}$ calculated by the cumulant analysis is in good agreement with $\overline{\langle R_h \rangle}_{z,app} = 690$ nm, which dominates the $G(\langle R_h \rangle_{z,app})$ curves in Figure 4a.

The cumulant analysis was also used to study the time evolution of $\langle R_h \rangle_{z,app}$ for a sample containing 0.5 wt % AAKLVFF and 20 wt % methanol at $\theta = 90°$. Figure 5 shows the results for the kinetic study, revealing a rapid self-assembly process of AAKLVFF which is stabilized after approximately 1 hour. Similarly, we reported[8] that a stabilization time of 1 hour was required to form nanotubes for 0.5 wt % AAKLVFF containing 100 wt % methanol. The data in Figure 5 supports the idea that $\overline{\langle R_h \rangle}_{z,app} = 690$ nm is associated with the fibril or the nanotube as a whole.

TEM and cryo-TEM results only gave a lower bound for the length of the self-assembled peptide structures. We used DLS as an alternative strategy to estimate the length of the peptide nanotubes or fibrils in solution. A cumulant analysis was used to calculate the initial decay rate $\langle \Gamma \rangle$ as a function of the scattering angle for 0.5 wt % AAKLVFF solutions containing different methanol contents at scattering angles of $40 \leq \theta \leq$

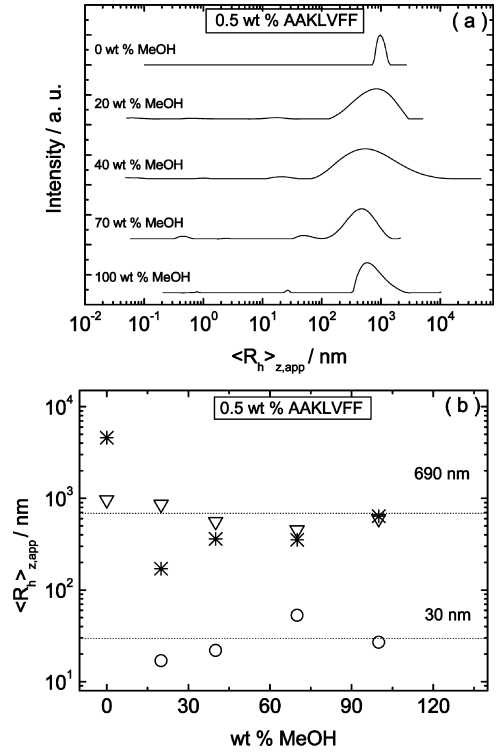

Figure 4. (a) Distributions of hydrodynamic radii calculated for 0.5 wt % AAKLVFF solutions containing 0−100 wt % methanol, using the constrained regularization method (scattering angle $\theta = 90°$). (b) (○), (▽) $\langle R_h \rangle_{z,app}$ measured from the distribution functions shown in (a) and (*) $\langle R_h \rangle_{z,app}$ calculated using the cumulant analysis. The broken lines indicate the average value $\overline{\langle R_h \rangle}_{z,app}$ obtained from the radii calculated using the constrained regularization method.

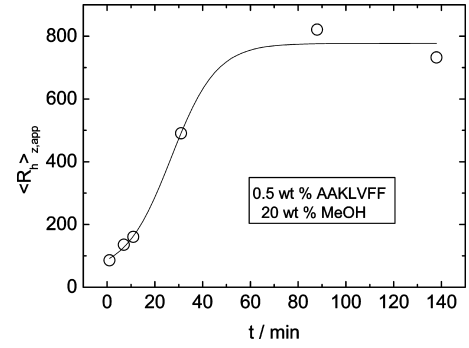

Figure 5. Time dependent evolution of the apparent hydrodynamic radius measured for a sample containing 0.5 wt % AAKLVFF and 20 wt % methanol (scattering angle of $\theta = 90°$). The solid line is a guide for the eyes.

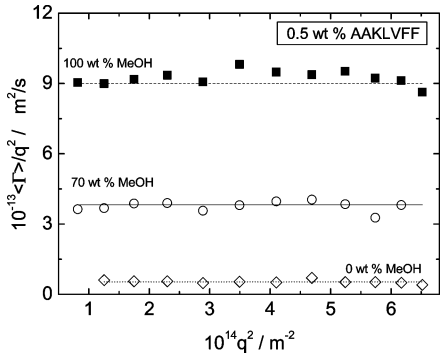

Figure 6. Diffusion coefficient data from DLS for 0.5 wt % AAKLVFF solutions containing 0−100 wt % methanol (as indicated in the figure), together with calculations according to eqs 5 and 6 for (• • •) [L_{DLS} = 85 μm, D_{cryo} = 18.5 nm]; (—) [L_{DLS} = 2.7 μm, D_{cryo} = 133.9 nm]; (- - -) [L_{DLS} = 3.2 μm, D_{cryo} = 85.5 nm].

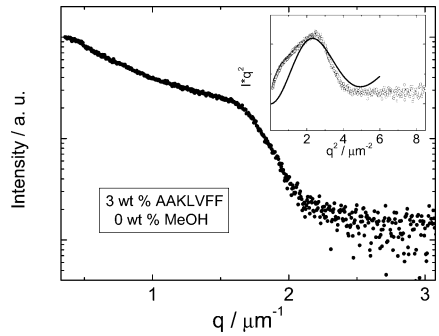

Figure 7. Static light scattering data for and aqueous solution of 3 wt % AAKLVFF. The inset corresponds to the Kratky representation of the same SLS data. The full line in the inset represents a fit to the peak position in the Kratky plot.

150°. Figure 6 shows the resulting q^2 dependence of $\langle\Gamma\rangle/q^2$. Figure 6 also shows the fitting of the experimental data according to eqs 5 and 6. The diameter (D) and the length (L_{DLS}) of the scattering object were the input and output parameters, respectively, used to fit eqs 5 and 6 to the experimental data in Figure 6. Table 1 lists the parameters used and calculated from the fits in Figure 6. The values of D were constrained to those obtained from cryo-TEM (D_{cryo}, Table 1) for the fibrils or nanotubes in solution. The flat tapes observed by cryo-TEM and TEM have been omitted in calculations with eqs 5 and 6 since those tapes have a wide distribution of dimensions.

The results in Table 1 show that L_{DLS} is in good agreement with L_{cryo} and L_{TEM} for 100 wt % methanol, while the same observation is not valid for samples containing 0 wt % methanol. This result is probably due to the flexibility of the objects self-assembled at 100 or 0 wt % methanol. Equations 5 and 6 are valid for rigid rods and therefore are appropriate to describe nanotubes (100 wt % methanol) but not to describe a system containing highly flexible fibers (0 wt % methanol).

Static light scattering was used to investigate the structure of a 3 wt % AAKLVFF solution (0 wt % methanol), in addition to the previous studies by TEM and DLS. Figure 7 shows the SLS profile, while the inset in Figure 7 shows the data presented in the form of a Kratky plot. Use of Kratky plots enables branched fibril network structures to be distinguished. The inset in Figure 7 shows a characteristic maximum in intensity, which suggests a branched fibril network with branch functionality of f = 12, a contour length of 1.5 μm, and a Kuhn length of 1.2 μm. (eq 3 in refs 23 and 24). This result is consistent with the information extracted from TEM experiments on samples with

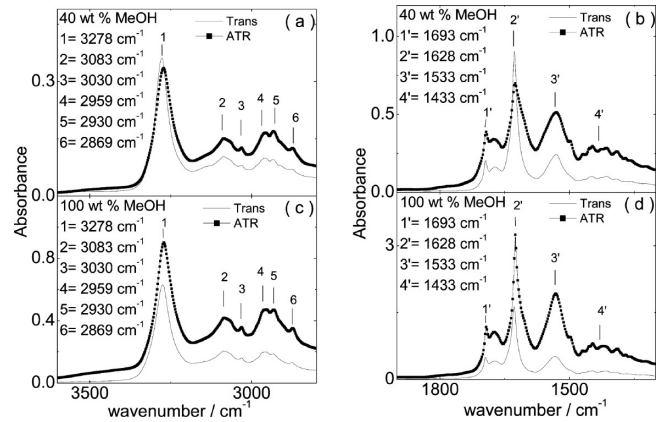

Figure 8. FT-IR spectra in the transmission and grazing incidence configurations obtained for a dried film of 1 wt % AAKLVFF in water, obtained for (a,b) 40 and (c,d) 100 wt % methanol.

0 wt % methanol (Figures 1 and 2), which indicated a contour length of several micrometers (Table 1).

Secondary Structure of AAKLVFF. The secondary structure was studied for films dried from 1 wt % AAKLVFF solutions containing 40−100 wt % methanol using FT-IR in transmission and grazing incidence modes. The comparison of transmission and grazing incidence FT-IR results has already been used by Hartgerink and co-workers[25] as a strategy to determine the orientation of the β-sheets with respect to the main axis of the fibril in β-sheet nanofibers of peptide amphiphiles. In addition, solutions containing AAKLVFF with varying amounts of methanol were also studied by FT-IR in transmission mode in order to provide information about possible drying effects through comparison with the corresponding spectra obtained for the dried films.

The features of the FT-IR spectra in transmission and grazing incidence modes obtained for the dried films were similar for 40−70 wt % methanol, while those features changed for 100 wt % methanol. Representative results for the dried films obtained from solutions containing 40 and 100 wt % methanol are shown in Figure 8.

Both the grazing incidence and transmission FT-IR data exhibit absorbance peaks at similar wavenumbers but with different intensities. FT-IR spectra in the amide I band are associated with a β-sheet structure.[26,27] The peaks at 1693 and 1628 cm^{-1} in Figure 8b,d correspond to the amide I band of the FT-IR spectra. In particular, the presence of the peak at 1628 cm^{-1} together with one at 1693 cm^{-1} suggests an antiparallel β-sheet arrangement.[26−29]

The peak at 1533 cm^{-1} is associated with the amide II band[27,30] and arises from the N−H in-plane bending or C−N stretching modes.[31] The peak at 1433 cm^{-1} might be a deformation of the CH_2 group expected at 1430−1460 cm^{-1}.[32,33]

Additional FT-IR peaks are located in the amide A band at 3278 cm^{-1} and amide B band at 3083 cm^{-1} (Figure 8a,c). An absorption peak at 3030 cm^{-1} is due to the stretching vibration from the benzene rings. A peak at 2959 cm^{-1} is due to the CH_3 vibration. A peak at 2930 cm^{-1} can be assigned to the CH_2 asymmetric stretching bands, while a peak at 2869 cm^{-1} is due to the CH_3 symmetric stretching bands.

As well as obtaining FT-IR data for dried films, spectra were measured for solutions. The obtained FT-IR spectra presented similar features in the amide I region, independent of the methanol content of the sample. Figure 9 shows representative results obtained in transmission mode for solutions containing 0 and 100 wt % methanol. Intermediate concentrations showed

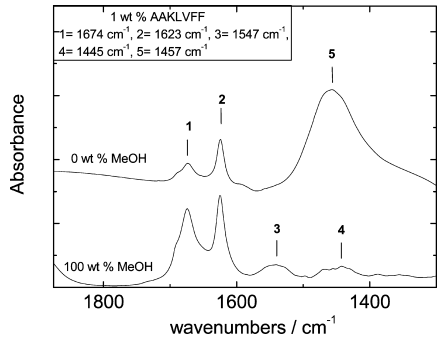

Figure 9. FT-IR spectra in the transmission configurations obtained for 1 wt % AAKLVFF solutions with 0 and 100 wt % methanol.

spectra with peaks in similar positions, and no systematic trend in peak intensities as a function of solvent composition was noted. The presence of two bands at 1674 and 1623 cm^{-1} for water and methanol solutions (Figure 9) reveals the formation of β-sheet structure in the fibrils and nanotubes in solution.[34,35] It can be inferred that any transition from fibril to nanotube is driven by a change in the arrangement of the β-sheets (as probed by the FT-IR study on dried films in different geometries) but not by alterations in the secondary structure.

Both the peak at 1445 cm^{-1} measured for pure methanol and the peak at 1457 cm^{-1} measured for pure water might be a deformation of the CH_2 group expected at 1430−1460 cm^{-1} (identified as 1433 cm^{-1} for the dried films in Figure 9).[32,33] The peak at 1547 cm^{-1}, measured for 100 wt % methanol (Figure 9), can be associated with the amide II band,[27,30] already discussed in relation to the dried films (Figure 8).

FT-IR experiments on solutions and dried films (Figures 8 and 9) show that the secondary structure is not altered by drying effects and therefore establish a correspondence between experiments made on peptide solutions and the corresponding dried films obtained from those solutions. These results are in good agreement with the outcome from TEM experiments (Figures 1 and 2).

CD experiments were undertaken on AAKLVFF solutions and dried films to obtain additional information on the secondary structure of the fibrils and nanotubes. Figure 10a shows the CD spectra obtained for AAKLVFF solutions containing 0, 50, and 100 wt % methanol. Figure 10b shows the CD spectra obtained for films dried from 1 wt % AAKLVFF solutions with 0, 20, and 100 wt % methanol (the CD spectrum for 0 wt % methanol was extracted from ref 9 as a reference).

The CD spectra in Figure 10a are characterized by a minimum in the range of 230−232 nm and a maximum at ∼215 nm. The negative band in the range of 230−232 nm can be associated with the minimum at 232 nm resulting from the stacking of aromatic amino acids due to peptide aggregation.[9,36−38] The maximum at 215 nm may be associated to a Cotton effect (n−π* transition).[39] A similar feature was noted for peptide FFKLVFF in solution.[7] Similar results to those shown in Figure 10a have been previously reported by us for solutions of AAKLVFF in water.[9] The spectra for the dried films are dominated by a minimum at 215 nm, which denotes a β-sheet structure.[40] The CD spectra for dilute peptide solutions are dominated by nonaggregated peptides. In contrast, CD data for the films dried from concentrated solutions show the fingerprint of the β-sheet structure, in good agreement with FT-IR data for the same films (Figure 8).

It is possible to model CD profiles for AAKLVFF with a positive maximum followed by a negative maximum, as discussed in the part 2 of this pair of papers. However, the

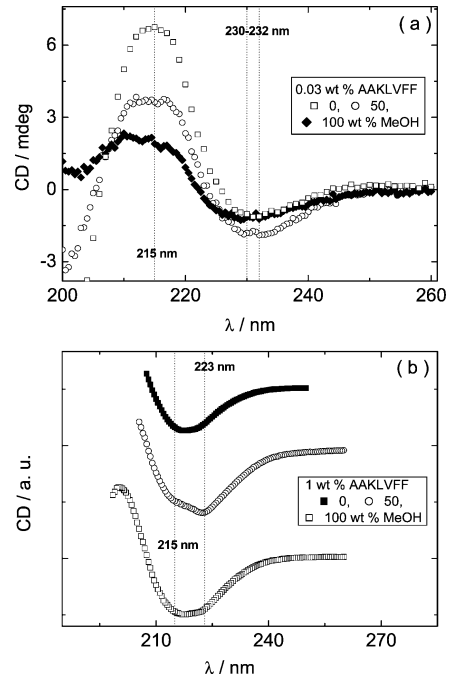

Figure 10. CD spectra for 0, 50, and 100 wt % methanol corresponding to (a) solutions containing 0.03 wt % AAKLVFF and (b) dried films obtained from solutions with 0.5 wt % peptide.

observed spectra are red-shifted by approximately 15 nm.[41] This might result from light scattering due to fibril formation, which cannot be accounted for in the model.

XRD was used to provide further evidence of amyloid fibril formation and to gain insight into the secondary structure. Samples were partially aligned by stretching the thread before the drying process started. The resulting XRD patterns obtained for films (prepared from 1 wt % AAKLVFF and 20−100 wt % methanol solutions) were characterized by two sharp reflections at 4.81 and 11.06 Å, corresponding to a well-defined "cross-β" pattern.[1] The XRD patterns had multiple orders of reflection, although they suggest that the degree of order is reduced for samples with higher methanol content. Two representative examples are shown in Figure 11 for 40 and 100 wt % methanol. The determination of the unit cell was performed using the software CLEARER.[42]

The results obtained for the indexation of the WAXS patterns in Figure 11 are listed in Table 2. Multiple solutions were possible, with similar χ^2 values. There was also some variability in repeat runs performed for stalks from 70 and 100 wt % methanol solutions. Nonetheless, it was possible to obtain a common consensus solution for the patterns with $b = 19.2 \pm 0.2$ Å and $c = 42 \pm 2$ Å; however, the unit cell dimension a was not well-defined. Solutions commonly involved multiples of the β-strand distance of 4.7−4.8 Å, as expected (Scheme 1), but were not uniquely defined, possibly due to twisting of the fibril about the fiber axis. The fact that a common solution exists indicates no systematic trend in unit cell parameters with water/methanol compositions and also indicates little effect of drying from solvents with different volatilities. The dimensions of the cell determined from data in Table 2 are similar to those reported by us previously for AAKLVFF in water, that is, $b = 18.6$ Å and $c = 43.7$ Å.[9]

It is possible to understand the values of the unit cell in terms of the AAKLVFF packing within the β-sheet. Within that frame, the cell axis a represents the peptide backbone separation within a β-sheet,[6] while the cell axis b corresponds to the spacing of

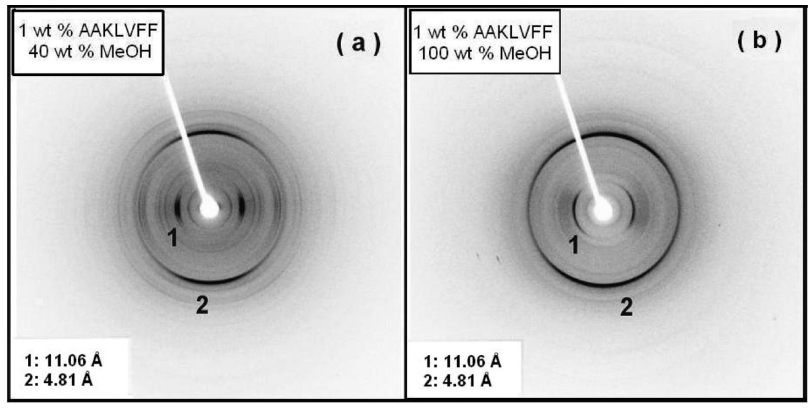

Figure 11. X-ray diffraction pattern from dried stalks prepared using a 1 wt % AAKLVFF solution for (a) 40 and (b) 100 wt % methanol. The tilted white line is the shadow of the beam stop.

TABLE 2: Calculated *d* Spacings and Cell Parameters Obtained from the Indexation of the XRD Patterns in Figure 11

wt % methanol	20	40	50	70	100
Equatorial Spacing/Å					
16.8−17.4	x		x	x	x
16.2		x			
11.0−11.7	x	x	x	x	x
10.35	x	x			
8.6−9.0		x	x		
8.40				x	
7.9−8.1		x			x
7.05−7.15	x	x		x	x
6.61		x	x		
6.49				x	
5.50−5.56	x	x	x	x	x
5.37		x			
5.13−5.19		x		x	x
4.32−4.38	x		x		x
4.0		x		x	x
3.9			x		x
3.1			x		x
Meridional Spacing/Å					
12.89	x				
8.94	x				
4.81	x	x	x	x	x
4.40		x		x	
4.06	x			x	
3.84		x			
3.70	x	x			

two β-sheets (with relatively small side groups and efficient packing).[6] Assuming that all of the peptide residues are in the β-sheet, the cell axis *c* corresponds to two AAKLVFF molecules (each AAKLVFF molecule is $7 \times 3.4 = 23.8$ Å long assuming a seven residue antiparallel β-sheet). The parameter *c* is slightly less than 2×23.8 Å, possibly indicating that terminal residues are not fully incorporated into the β-sheet structure or possibly that there are some parallel β-sheets (which give $7 \times 3.2 = 22.4$ Å long conformers). Scheme 2 shows a proposed model for the arrangement of the AAKLVFF β-sheets within the unit cell.

The dimensions of the unit cell parameters are at least 1 order of magnitude smaller than the size of the parameters measured from HR-TEM and discussed at the beginning of this section (Table 1, Figures 1−3). It appears therefore that the fibrils and nanotubes observed in TEM are higher-order aggregates containing multiple repeats of the unit cell *b* and *c* axes orthogonal to the fibril or nanotube (*a*) axis.

The data extracted from the XRD analysis can be correlated to the FT-IR data on dried films (Figure 8) in order to obtain additional information regarding the orientation of the β-strands making the fibrils or nanotubes. The features in the amide I region in Figure 8 provide evidence of β-sheet structure. The relative intensity of the amide I peaks with respect to the amide II band peaks, I_r, is a fingerprint of the β-sheet orientation with respect to the incident beam. Figure 8 shows that I_r is attenuated in the ATR geometry for films corresponding to 40 wt % methanol.[9] In contrast, the situation is inverted for films prepared from 100 wt % methanol solutions, where I_r is enhanced in the ATR geometry.

Hartgerink and co-workers[25] provided a model for the orientation of the β-sheet C═O bonds with respect to the fibril axis as a function of I_r. They show that I_r is attenuated in the grazing incidence geometry when the IR laser beam is oriented parallel to the amide C═O bonds (Scheme 2i), and these are simultaneously oriented along the fibril axis, leading to a configuration in which the β-strands are aligned perpendicular to the main axis of the fibril (it is not possible to determine from FT-IR whether they are also twisted). Conversely, when C═O bonds are perpendicular to the IR laser beam, I_r is enhanced in the grazing incidence geometry.[25] This is consistent with a radial arrangement of β-strands around the fibril axis, leading to a nanotube structure based on "wrapped β-sheets" (Scheme 2ii). The models depicted in Scheme 2 are in agreement with previous results from X-ray diffraction, which show orientation with meridional peaks from the 4.8 Å interstrand separation (Figure 11a). The same orientation is also observed for nanotube samples (Figure 11b).

According to this model (Scheme 2), the results in Figure 8c,d indicate that the orientation of the C═O bonds discontinuously changes from parallel (20−70 wt % methanol) to perpendicular (100 wt % methanol) to the IR beam, in correlation with the transition from fibril to nanotube observed when the methanol content of the sample increases from 70 to 100 wt %.

Proposed mechanisms for the self-assembly of AAKLVFF in water/methanol mixtures are discussed in part 2 of this series,[41] which concerns molecular dynamics computer simulations as well as ROESY NMR measurements to determine molecular conformation. At a molecular level, self-assembly is driven by a combination of hydrogen bonding within the β-sheet and hydrophobic and electrostatic interactions of the side chains between β-sheets. The β-strands in AAKLVFF appear to have an antiparallel arrangement to give 0 net charge and dipole, considering the charged termini alone. This is consistent with the observations from FT-IR and X-ray diffraction. It has also to be considered that the lysine residue is charged and the charge

SCHEME 1: Model for the Packing of AAKLVFF Antiparallel β-Sheets in an Orthorhombic Cubic Cell, Showing the Unit Cell Parameters According to the XRD Results Listed in Table 1[a]

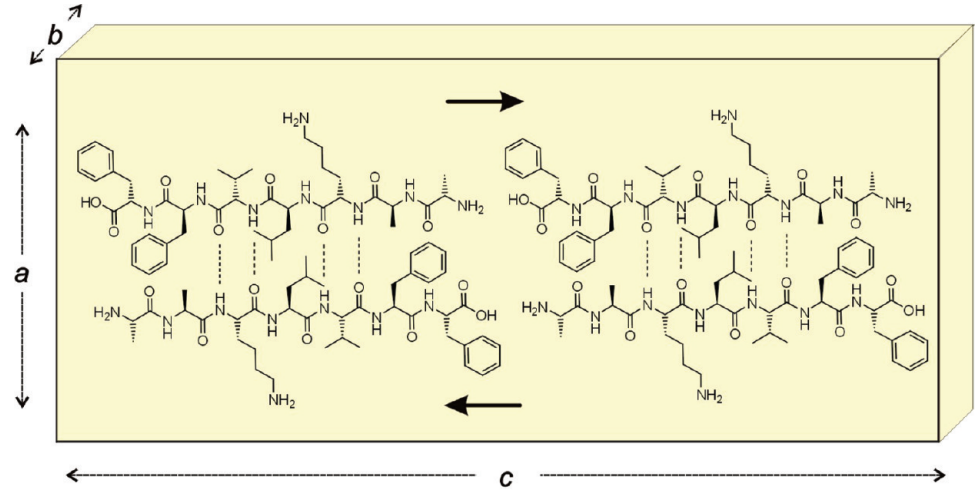

[a] The (antiparallel) packing of the β-sheets agrees with FT-IR data.

SCHEME 2: Sketch Showing Orientation with Respect to the IR Beam of β-Strands (short solid lines) and Hydrogen Bonds along C═O Bond Directions (short dashed lines)[25] in (i) Twisted Fibrils and (ii) Nanotubes (not drawn to scale)

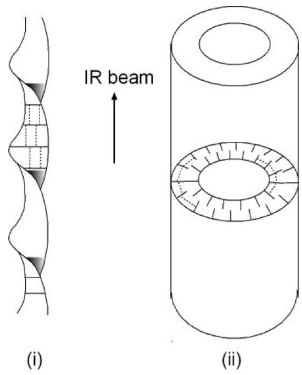

is off of the strand axis, giving rise to net charge and dipole moment. The relative strength of dipolar and charge (monopolar) interactions depends on the solvent permittivity. There is therefore a change in solvent permittivity when the methanol fraction in the water/methanol mixtures is increased to 100 wt % methanol (relative dielectric constant of water $\chi_r = 88$ and methanol $\chi_r = 30$, at 20 °C and 1 kHz). Packing constraints due to electrostatic interactions and also aromatic stacking interactions of phenylalanine are also important in that these govern the side-chain packing that controls stacking of β-sheets. However, we tentatively ascribe the different modes of self-assembly in water or methanol mainly to the influence of solvent on hydrogen bonding within the β-sheets. This has recently been investigated via statistical mechanics calculations compared to data for poly(*N*-isoproylacrylamide) in water/methanol mixtures.[43] These reveal a collapse in chain dimensions around a 50/50 water/methanol composition. Similarly, poly(ethylene oxide) shows a minimum in viscosity at a 2:1 water/methanol ratio, and this could be interpreted using Tanaka's model for the chain dimensions and fractional chain coverage by solvent.[44] We believe that competitive hydrogen bonding to water or methanol drives the distinct self-assembled motifs in AAKLVFF in water/methanol mixtures due to changes in the arrangement of β-strands within the β-sheets. Twisted fibril structures have been observed and analyzed by several groups,[45−48] and peptide nanotubes have been observed and modeled also.[12,48,49] It has been proposed that the nanotubes result from helical ribbon structures that close into tubes,[12] helical ribbon structures themselves also being observed.[38,50,51] However, we are not aware of a report on a system that exhibits a transformation between twisted fibrils and nanotubes, dependent on the solvent. Part 2 of this study discusses our modeling in detail. It is possible to account for both twisted fibril and nanotube structures using molecular dynamics simulations. The dimensions of the aggregates are compared to those reported here, determined experimentally. The orientation of the strands within the self-assembled structures is also investigated. The molecular conformation of isolated molecules in dilute solution is obtained from ROESY 2D-NMR experiments. CD spectra are computed using software based on a protein structure database.

4. Summary

The self-assembly of AAKLVFF in mixtures of water/methanol has been studied. This builds on our previous work on AAKLVFF in methanol and water solutions, for which nanotube[8] and fibril[9] formation is observed, respectively. TEM clearly shows peptide fibrils and tapes for low methanol contents, while the formation of peptide nanotubes can be detected for 100 wt % methanol solutions. Tapes predominate for 50−70 wt % methanol; this is close to the composition previously reported to lead to anomalies in chain dimensions or viscosity for polymers in water/methanol mixtures. It suggests that competitive hydrogen bonding may cause disruption of the twisted fibril and nanotube structures in the pure solvents. The intermediate structure comprises broad and polydisperse tapes, which appear to form from lateral aggregation of thin protofilaments. These transformations may result from changes in the hydrogen bonding pattern within the β-sheets. Electrostatic and hydrophobic stacking interactions of side chains may also be important.

FT-IR spectroscopy shows that the transition from fibril to nanotube geometry is driven by the spatial rearrangement of the β-sheets, without a change in the secondary structure. A comparison of FT-IR in transmission and in reflectance (FT-IR beam in different orientations with respect to the sample plane) indicates that the C═O bonds are parallel to the axis of twisted fibrils but perpendicular to the axis of the nanotubes. The β-sheet secondary structure of the fibrils and nanotubes was confirmed

by CD. This also shows that in dilute solution, the spectra do not exhibit the canonical form for β-sheets but contain important contributions from aromatic stacking interactions. Dried films show the classic form, with a maximum at around 195 nm and a minimum at 215 nm. The FT-IR and CD results were supported by XRD data, which provided quantitative information on the packing of the AAKLVFF peptide into β-strands.

We propose that competitive hydrogen bonding in water/methanol mixtures provides a key driving force in the self-assembly process. It leads to differences in the stacking of the β-strands within the β-sheets. This will also be influenced by hydrophobic and electrostatic interactions, which affect the stacking of β-sheets due to side-chain interaction. AAKLVFF is a remarkable system to examine these effects, and future work will focus on the rational design of related variants to further probe the interplay of these forces and hence to tune the self-assembled structures.

Acknowledgment. We thank Dr. Rebecca Green (Department of Pharmacy, University of Reading) for access to the FT-IR instrument and Dr. Louise C. Serpell (Department of Biochemistry, University of Sussex) for providing a copy of the software CLEARER. We are grateful to Dr. David Nutt (University of Reading) for stimulating discussions in regard to modelling.

References and Notes

(1) Goedert, M.; Spillantini, M. G. *Science* **2006**, *314*, 777–781.
(2) Hamley, I. W. *Angew. Chem., Int. Ed.* **2007**, *46*, 8128–8147.
(3) Gras, S. L.; Tickler, A. K.; Squires, A. M.; Devlin, G. L.; Horton, M. A.; Dobson, C. M.; MacPhee, C. E. *Biomaterials* **2008**, *29*, 1553–1562.
(4) Chiti, F.; Dobson, C. M. *Annu. Rev. Biochem.* **2006**, *75*, 333–366.
(5) Soto, C.; Sigurdsson, E. M.; Morelli, L.; Kumar, R. A.; Castano, E. M.; Frangione, B. *Nat. Med.* **1998**, *4*, 822–826.
(6) Krysmann, M. J.; Castelletto, V.; Kelarakis, A.; Hamley, I. W.; Hule, R. A.; Pochan, D. J. *Biochemistry* **2008**, *47*, 4597–4605.
(7) Krysmann, M. J.; Castelletto, V.; Hamley, I. W. *Soft Matter* **2007**, *2*, 1401–1406.
(8) Krysmann, M. J.; Castelletto, V.; McKendrick, J. E.; Clifton, L. A.; Hamley, I. W.; Harris, P. J. F.; King, S. M. *Langmuir* **2008**, *24*, 8158–8162.
(9) Castelletto, V.; Hamley, I. W.; Harris, P. J. F. *Biophys. Chem.* **2008**, *138*, 29–35.
(10) Mehta, A. K.; Lu, K.; Childers, W. S.; Liang, Y.; Dublin, S. N.; Dong, J. J.; Snyder, J. P.; Pingali, S. V.; Thiyagarajan, P.; Lynn, D. G. *J. Am. Chem. Soc.* **2008**, *130*, 9829–9835.
(11) Liang, Y.; Pingali, S. V.; Jogalekar, A. S.; Snyder, J. P.; Thiyagarajan, P.; Lynn, D. G. *Biochemistry* **2008**, *47*, 10018–10026.
(12) Dong, J. J.; Lu, K.; Lakdawala, A.; Mehta, A. K.; Lynn, D. G. *Amyloid* **2006**, 206–215.
(13) Petkova, A. T.; Leapman, R. D.; Guo, Z. H.; Yau, W. M.; Mattson, M. P.; Tycko, R. *Science* **2005**, *307*, 262–265.
(14) Krishnan, R.; Lindquist, S. L. *Nature* **2005**, *435*, 765–772.
(15) Talmon, Y. *Ber. Bunsen-Ges. Phys. Chem.* **1996**, *3*, 364–372.
(16) Berne, B. J.; Pecora, R. *Dynamic Light Scattering*; Wiley-Interscience: New York, 1976.
(17) Provencher, S. W. *Comput. Phys. Commun.* **1982**, *27*, 229–242.
(18) Thompson, J. W.; Kaiser, T. J.; Jorgenson, J. W. *J. Chromatogr., A* **2006**, *1134*, 201–209.
(19) Shen, C.-L.; Scott, G. L.; Merchant, F.; Murphy, R. M. *Biophys. J.* **1993**, *65*, 2383–2395.
(20) Maeda, T.; Fujime, S. *Macromolecules* **1984**, *17*, 1157–1167.
(21) Russo, P. S.; Karasz, F. E.; Langley, K. H. *J. Chem. Phys.* **1984**, *80*, 5312–5325.
(22) Castelletto, V.; Hamley, I. W. *Polym. Adv. Technol.* **2006**, *17* (3), 137–144.
(23) Shen, C.-L.; Murphy, R. M. *Biophys. J.* **1995**, *69*, 640–651.
(24) Pallitto, M. M.; Ghanta, J.; Heinzelman, P.; Kiessling, L. L.; Murphy, R. M. *Biochemistry* **1999**, *38*, 3570–3578.
(25) Paramonov, S. E.; Jun, H. W.; Hartgerink, J. D. *J. Am. Chem. Soc.* **2006**, *128*, 7291–7298.
(26) Haris, P.; Chapman, D. *Biopolymers* **1995**, *37*, 251–263.
(27) Stuart, B. *Biological Applications of Infrared Spectroscopy*; Wiley: Chichester, U.K., 1997.
(28) Rösler, A.; Klok, H.-A.; Hamley, I. W.; Castelletto, V.; Mykhaylyk, O. O. *Biomacromolecules* **2003**, *4*, 859–863.
(29) Miyazawa, T.; Blout, E. R. *J. Am. Chem. Soc.* **1961**, *83*, 712–719.
(30) Lin, S.-Y.; Chu, H.-L. *Int. J. Biol. Macromol.* **2003**, *32*, 173–177.
(31) Sarkar, S.; Chourasia, A.; Maji, S.; Sadhukran, S.; Kumar, S.; Adhikari, B. *Bull. Mater. Sci.* **2006**, *29*, 475–484.
(32) Benaki, D. C.; Aggeli, A.; Chryssikos, G. D.; Yiannopoulos, Y. D.; Kamitsos, E. I.; Brumley, E.; Case, S. T.; Boden, N.; Hamodrakas, S. J. *Int. J. Biol. Macromol.* **1998**, *23*, 49–59.
(33) Krimm, S.; Bandekar, J. *Adv. Protein Chem.* **1986**, *38*, 181–364.
(34) Chiti, F.; Webster, P.; Taddei, N.; Clark, A.; Stefani, M.; Ramponi, G. *Proc. Natl. Acad. Sci. U.S.A.* **1999**, *96*, 3590–3594.
(35) Muga, A.; Arrondo, J. L. R.; Bellon, T.; Sancho, J.; Bernabeu, C. *Arch. Biochem. Biophys.* **1993**, *300*, 451–457.
(36) Reshetnyak, Y. K.; Segala, M.; Andreev, O. A.; Engelman, D. M. *Biophys. J.* **2007**, *93*, 2363–2372.
(37) Roy, R. S.; Gopi, H. N.; Raghothama, S.; Gilardi, R. D.; Karle, I. L.; Balaram, P. *Biopolymers* **2005**, *80*, 787–799.
(38) Castelletto, V.; Hamley, I. W.; Hule, R. A.; Pochan, D. J. *Angew. Chem.* **2009**, *48*, 2317–2320.
(39) Sun, S. F. *Physical Chemistry of Macromolecules: Basic Principles and Issues*; John Wiley & Sons: London, 2004, p. 275.
(40) Kelly, S. M.; Jess, T. J.; Price, N. C. *Biochim. Biophys. Acta* **2005**, *1751*, 119–139.
(41) Hamley I. W.; Nutt, D.; Brown, G. D.; Miravet, J. F.; Escuder, B. 2009, in preparation.
(42) Makin, O. S.; Atkins, E.; Sikorski, P.; Johansson, J.; Serpell, L. C. *Proc. Natl. Acad. Sci. U.S.A.* **2005**, *102*, 315–320.
(43) Tanaka, F.; Koga, T.; Winnik, F. M. *Phys. Rev. Lett.* **2008**, 101.
(44) Shankar, R.; Klossner, R. R.; Weaver, J. T.; Koga, T.; van Zanten, J. H.; Krause, W. E.; Colina, C. M.; Tanaka, F.; Spontak, R. J. *Soft Matter* **2009**, *5*, 304–307.
(45) Benzinger, T. L. S.; Gregory, D. M.; Burkoth, T. S.; Miller-Auer, H.; Lynn, D. G.; Botto, R. E.; Meredith, S. C. *Biochemistry* **2000**, *39*, 3491–3499.
(46) Aggeli, A.; Nyrkova, I. A.; Bell, M.; Harding, R.; Carrick, L.; McLeish, T. C. B.; Semenov, A. N.; Boden, N. *Proc. Natl. Acad. Sci. U.S.A.* **2001**, *98*, 11857–11862.
(47) Fishwick, C. W. G.; Beevers, A. J.; Carrick, L. M.; Whitehouse, C. D.; Aggeli, A.; Boden, N. *Nano Lett.* **2003**, *3*, 1475–1479.
(48) Lu, K.; Jacob, J.; Thiyagarajan, P.; Conticello, V. P.; Lynn, D. G. *J. Am. Chem. Soc.* **2003**, *125*, 6391–6393.
(49) Valery, C.; Paternostre, M.; Robert, B.; Gulik-Krzywicki, T.; Narayanan, T.; Dedieu, J. C.; Keller, G.; Torres, M. L.; Cherif-Cheikh, R.; Calvo, P.; Artzner, F. *Proc. Natl. Acad. Sci. U.S.A.* **2003**, *100*, 10258–10262.
(50) Pagel, K.; Wagner, S. C.; Samedov, K.; von Berlepsch, H.; Bottcher, C.; Koksch, B. *J. Am. Chem. Soc.* **2006**, *128*, 2196–2197.
(51) Rubin, N.; Perugia, E.; Goldschmidt, M.; Fridkin, M.; Addadi, L. *J. Am. Chem. Soc.* **2008**, *130*, 4602.

JP902860A